High-temperature a.c. electrical behaviour of polycrystalline calcium zirconate

C. C. WANG, W. H. CHEN*, S. A. AKBAR
Department of Materials Science and Engineering, The Ohio State University, Columbus, OH 43210, USA

M. A. ALIM
The Ohio Brass Company, Hubbell Inc., Wadsworth, OH 44281, USA

The a.c. electrical response of undoped polycrystalline calcium zirconate was evaluated at elevated temperatures ($900 \leqslant T \leqslant 1400\,^{\circ}C$) in air as a function of frequency in the range 5 Hz to 13 MHz. A systematic analysis of the a.c. electrical data revealed semicircular relaxation(s) in the impedance, admittance and modulus planes. An equivalent circuit model, representing grain and grain-boundary regions, is proposed. This circuit can be transformed to another representation which incorporates a possible trapping effect across the grain boundaries. The equivalence of these two representations is demonstrated by examining the correspondence between the two sets of circuit elements without resorting to empirical distributed-element models.

1. Introduction

There is a growing interest in calcium zirconate-based oxides for potential sensor/device applications at elevated temperatures. In particular, several studies have been reported on the use of calcium zirconate-based systems for monitoring oxygen [1–3], humidity and hydrogen [4–6]. In these studies, sintered polycrystalline samples were used to characterize carrier types and the concentrations of ionic (proton or oxygen) and electronic charge carriers as a function of temperature, impurity distribution, and oxygen and/or water vapour partial pressures. Pretis *et al.* [7] reported that undoped calcium zirconate ($CaZrO_3$) is a p-type semiconductor in air. When doped with oxides such as Al_2O_3, Y_2O_3 and MgO or with a small excess of ZrO_2 or CaO, it becomes predominantly an oxygen-ion conductor [1, 2, 7–10]. For a sample doped with trivalent cations such as indium, scandium and gallium, it may become predominantly a proton conductor when exposed to a hydrogen-containing atmosphere (steam) at temperatures ranging from 600–1000 °C [4, 5]. The protonic conduction, however, tends to diminish at higher temperatures and can be replaced by electronic (hole) conduction, especially in a dry atmosphere [4].

To optimize the performance of a polycrystalline-based device, it is vital to understand the contributions of grains, grain boundaries, additional phases, defect states therein, possible electrode-effect (due to the mismatch in the work function at the device/electrode interface or gas–solid reactions), etc. These characteristics can be studied via immittance (impedance or admittance) measurements under varying experimental conditions such as temperature, electrical stress, etc. These immittance data can then be analysed using the lumped parameter/complex plane (LP/CPA) technique. This technique has proved to be a viable route for characterizing the electrical behaviour of heterogeneous devices [11–27]. A systematic analysis of the immittance data (e.g. as a function of temperature) using the LP/CPA technique, can reveal the degree of structural uniformity, type of charge carrier, variation in the electrical conduction path, degradation, time-dependent behaviour leading to ageing, etc. [11–13]. This paper reports the a.c. electrical behavior of undoped polycrystalline $CaZrO_3$ in the temperature range 900–1400 °C.

2. Experimental procedure

The samples used in this study were prepared from Johnson Matthey Puratronic high-purity (99.99%) powders: calcium carbonate ($CaCO_3$ with 20 p.p.m. Mg and 5 p.p.m. Fe) and zirconium oxide (ZrO_2 with 1 p.p.m. Fe and Si). These powders were mixed in stoichiometric ratio and ball-milled using zirconia balls in isopropyl alcohol for 24 h to achieve a uniform distribution of particle size of about 1 μm. The slurry was dried at 120 °C for 6 h and powdered in a mortar. The powder mixture was then calcined between 1000 and 1400 °C in air for 12 h followed by grinding after cooling to room temperature. This process was repeated at least twice to ensure homogeneous mixing and complete solid-state reaction. The calcined powder

* Present address: Orton Ceramic Foundation, 6991 Old 3C Highway, Westerville, OH, USA.

0022–2461

was then used to prepare disc-shaped samples (9 mm diameter and 1.5 mm thick) by cold-pressing at 5000 p.s.i. (10^3 p.s.i. = 0.89 N mm^{-2}) for 2 min followed by sintering in air at 1550 °C for 48 h. Each sintered samples was found to be about 95% theoretical density with an average grain size of about 10 μm.

For electrical measurements, the opposite flat faces of the disc were polished and painted with a thin layer of platinum paste (Engelhard 3788) to form the electrodes. After the organic binder in the paste was dried in air at room temperature for 24 h, the assembly was cured at 1200 °C for 24 h. Successive layers of paste were applied as necessary to ensure a uniform contact at the electrode. In all measurements, the electrode area and the distance between the electrodes (i.e. sample thickness) were kept as identical as possible.

Both the two-probe and four-probe measurement techniques were used to obtain the electrical resistance. There was no observable difference in the measured resistance between the two techniques. The data reported in this paper are based on the two-probe method. The acquisition of the two-probe a.c. (amplitude of about 1 V) electrical data in the frequency range 5 Hz to 13 MHz was accomplished by an impedance analyser (Model HP4192A, Hewlett–Packard, Tokyo, Japan). The data, in the form of the terminal admittance, were obtained by averaging at least five measurements at a given frequency to minimize the noise. The data acquisition was fully automated by interfacing the analyser with a computer. Necessary electrical parameters associated with semicircular relaxations were extracted independently using complex non-linear least squares (CNLS) curve-fitting software developed in the authors' laboratory at The Ohio State University. In the fitting, the depression angle, θ, and time constant, τ were determined independently. Depending on the complex plane of analysis, either the resistance, R, or the capacitance, C, components of a semicircular relaxation was independently extracted. In the Z*-plane, for example, the time constant and its resistance component were obtained independently from CNLS fitting and then the relation, $\tau = RC$, was used to obtain the capacitance.

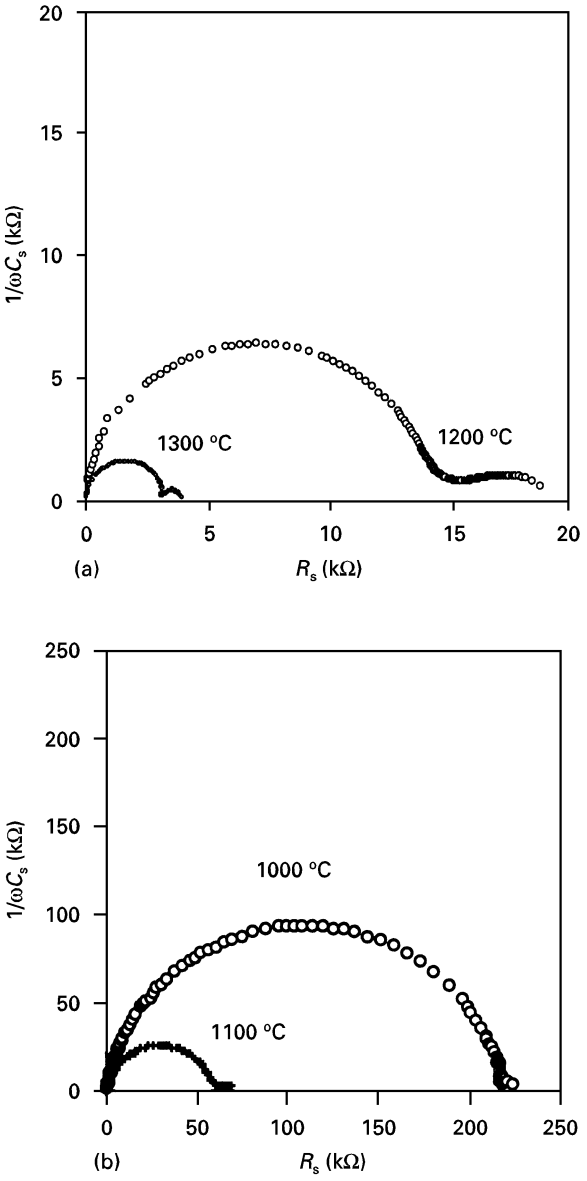

Figure 1 Impedance plots of a calcium zirconate sample at various temperatures.

3. Analysis of immittance data

The a.c. electrical data obtained were representable in three complex planes (Z*, Y*, and M*), similar to previously observed for polycrystalline yttria [21, 22]. In the Z*-plane, only one semicircular relaxation was visible at temperatures below 1100 °C. At higher temperatures, a second semicircle emerged in the low-frequency region, as shown in Fig. 1. When the same data were displayed in the M*-plane, a single-relaxation-like semicircle was obtained at all temperatures ($900 \leqslant T \leqslant 1400$ °C), as depicted in Fig. 2a. At high temperatures, however, there is an inflection in the M*-plane in the low-frequency range, which matches the emergence of the low-frequency relaxation in the Z*-plane. As highlighted in Fig. 2b, this inflection is the demarcation between the two semicircular relaxations in the Z*-plane. When presented in the Y*-plane, the same data yield a highly depressed semicircle in the low-frequency region and a nearly vertical line at the high-frequency region as depicted in Fig. 3. It is interesting to note that the demarcation in the frequency domain for the Y* plane representation between the two consecutive responses is the same as those observed in the Z*- and M*-plane plots. As the low-frequency semicircular relaxations in the Z*- and Y*-planes were only partially visible and thus not fully resolvable at low temperatures, the electrical parameters associated with these relaxations were extracted at high temperatures (i.e. $1100 \leqslant T \leqslant 1400$ °C). A complete set of the extracted parameters from the three complex planes is summarized in Table I.

4. Results and discussion

The relaxation represented by the time-constant, τ_1, obtained in the high-frequency semicircle in the Z*-plane (Fig. 1) is thermally activated as shown in Fig. 4. The activation energy, E_{τ_1}, of this relaxation is found

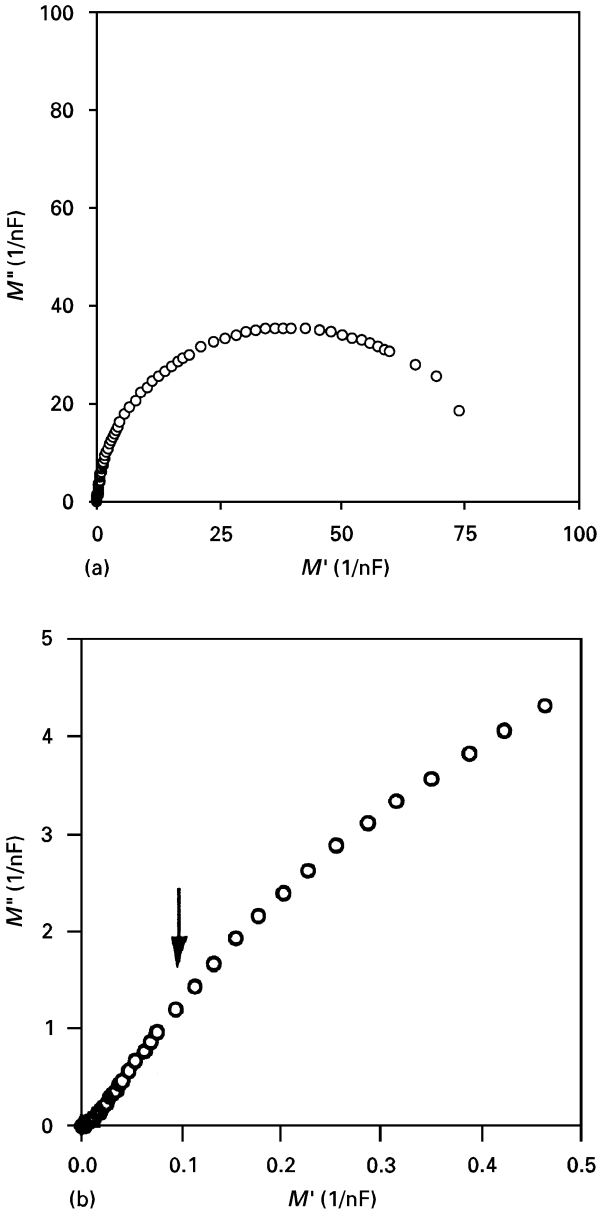

Figure 2 (a) The modulus plot of the same sample as in Fig. 1 at 1200 °C. (b) The demarcation between high- and low-frequency regions marked with an arrow.

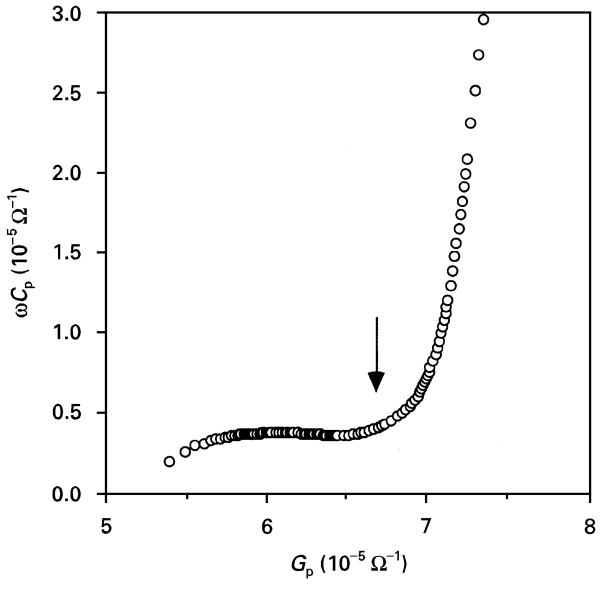

Figure 3 Admittance plot of the same sample as in Fig. 1 at 1200 °C.

TABLE I Equivalent circuit parameters as obtained from semicircular relaxations observed in the impedance, modulus and admittance planes for $CaZrO_3$ at 1200 °C

Impedance plane							Admittance plane					Modulus plane			
τ_1 (s)	R_1 (Ω)	C_1 (F)	θ_1 (deg)	τ_2 (s)	R_2 (Ω)	C_2 (F)	θ_2 (deg)	τ^Y (s)	R^Y (Ω)	C^Y (F)	θ^Y (deg)	C_∞ (F)	R_0 (Ω)	R_1^Y (Ω)	τ_1^M (s)	R_1^M (Ω)	C_1^M (F)	θ_1^M (deg)
1.86×10^{-7}	1.37×10^{4}	1.36×10^{-11}	4.6	1.69×10^{-3}	5.42×10^{3}	3.12×10^{-7}	46	6.79×10^{-4}	4.66×10^{4}	1.46×10^{-8}	50	1.42×10^{-11}	2.00×10^{4}	1.35×10^{4}	1.73×10^{-7}	1.31×10^{4}	1.32×10^{-11}	3.7

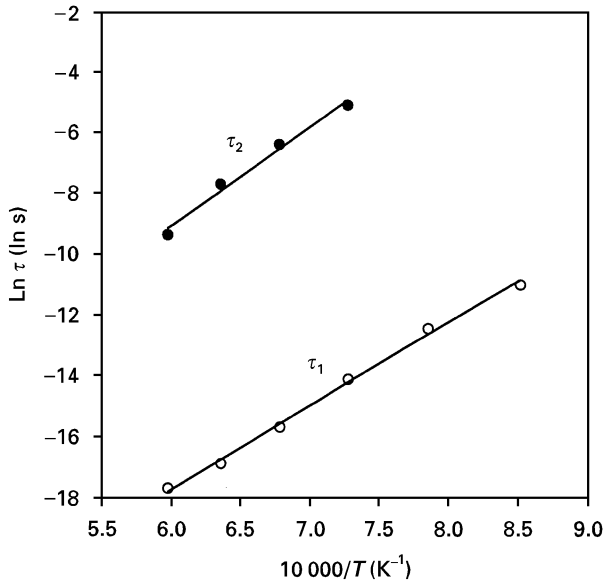

Figure 4 Temperature dependence of the relaxation times, τ_1 and τ_2, associated with the high- and low-frequency semicircles, respectively, in the Z*-plane.

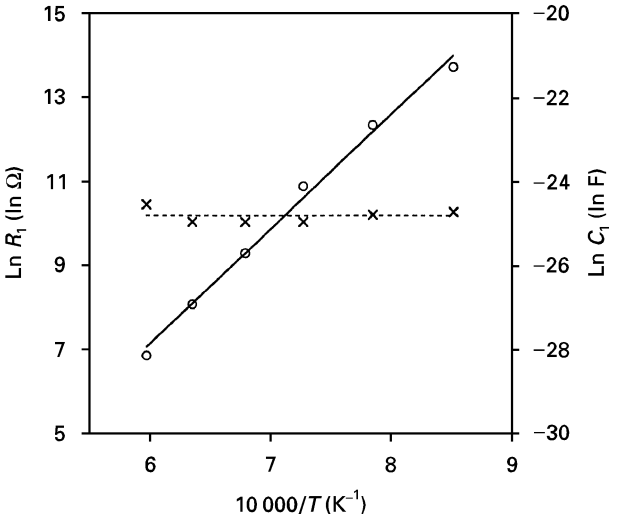

Figure 5 Temperature dependence of (○) the resistance, R_1, and (×) capacitance, C_1, associated with the high-frequency semicircular relaxation in the Z*-plane.

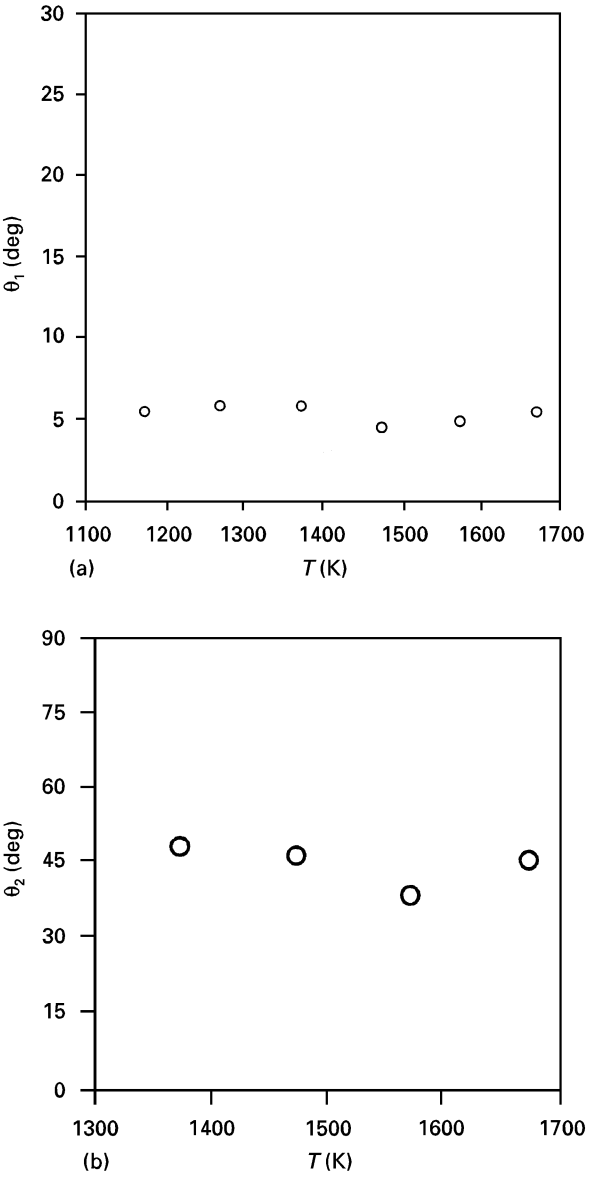

Figure 6 Temperature dependence of the depression angles, θ_1 and θ_2.

to be 2.36 eV. The temperature dependence of its constituting components, R_1 and C_1 ($\tau_1 = R_1C_1$), are also examined and the results are shown in Fig. 5. The resistance, R_1, exhibits a temperature dependence with an activation energy of 2.36 eV (E_{R_1}), matching that of τ_1. This matching reveals the invariant nature of capacitance C_1 in the same temperature range, as shown in Fig. 5.

The high-frequency semicircular relaxation was found to exhibit a finite depression angle, θ_1, of about 5°, which remains nearly constant (Fig. 6) within the temperature range of this study ($900 \leqslant T \leqslant 1400\,^{\circ}C$). This means that in this temperature range the relaxation remains nearly ideal (Debye-like) and the associated conduction process experiences a small degree of heterogeneity in the material.

The temperature dependence of the low-frequency relaxation, τ_2, is also shown in Fig. 4. The activation energy (E_{τ_2}) of τ_2 is 2.78 eV. Fig. 7 shows the temperature dependence of R_2 and C_2 associated with $\tau_2 (= R_2C_2)$. Again, the activation energy of τ_2 matches that of R_2 ($E_{\tau_2} \simeq E_{R_2} = 2.79$ eV), yielding a temperature-independent C_2. However, this low-frequency semicircular relaxation is characterized with a large depression angle, $\theta_2 (\approx 45\,^{\circ})$, as shown in the inset of Fig. 6. It indicates a non-Debye relaxation with significant degree of heterogeneity in the conduction path. The degree of heterogeneity, however, remains nearly the same in the temperature range between 1100 and 1400 °C.

The difference in the activation energies of R_1 and R_2 (or τ_1 and τ_2) indicates that the charge migration associated with R_1 and R_2 occurred by different processes. The values of C_1 and C_2 (14 pF and 30 μF) suggest that the corresponding relaxations may be associated with grains and grain-boundaries, respectively. It is possible that close to a grain boundary, the transport properties are controlled by impurities, which are expected to be present there in higher concentration than in the grain. This gives rise

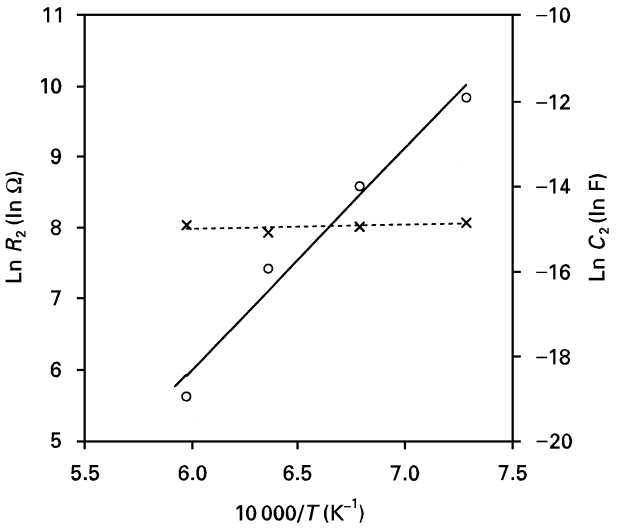

Figure 7 Temperature dependence of (○) the resistance, R_2, and (×) capacitance, C_2, associated with the low-frequency semicircular relaxation in the Z*-plane.

to a distinct and relatively high C_2 and, thus, a separate relaxation process in the Z*-plane at low frequencies.

It is important to note that in the Z*-plane, the low-frequency relaxation was not observed at temperatures $< 1100\,^{\circ}C$ (Fig. 1). This can be attributed either to a *lumped* behaviour (inseparable relaxations) or to the limitation in the low-frequency limit of the HP4192A impedance analyser ($f \geqslant 5$ Hz). The former is possible only when the relaxation time constants become similar at lower temperatures. This is obviously not the case for calcium zirconate as indicated in Fig. 4. From Fig. 4, it is expected that the time constants remain significantly different at temperatures below 1100 °C. Therefore, it is concluded that the low-frequency relaxation was not observed at temperatures below 1100 °C owing to the low-frequency limit of the impedance analyser.

In perovskite-type oxides, the type of charge carriers responsible for the occurrence of the two semicircles in the Z*-plane may be either ionic or electronic. Earlier studies seem to support a predominantly p-type conduction for perovskite zirconates at high oxygen partial pressures [7, 30, 31]. Pretis *et al.* [7] have reported a predominantly p-type conduction in undoped polycrystalline $CaZrO_3$. In fact, conductivity isotherm measurements on our calcium zirconate samples indicated a p-type conduction, as the electrical conductivity was found to increase with oxygen partial pressure [22]. In addition, no difference was found in the electrical conductivities measured in wet and dry air. These results suggest a predominantly p-type conduction in the undoped yttria, possibly originating from the presence of impurities (acceptors) in the samples [4].

The low-frequency response in the M*-plane was not resolved through the curve-fitting procedure, as it is heavily overlapped with the high-frequency response. Therefore, only the high-frequency response in the form of a semicircle locus was evaluated. The analysis of the high-frequency semicircle provided a resistance R_1^M, a capacitance C_1^M and the corresponding relaxation time $\tau_1^M(\tau_1^M = R_1^M C_1^M)$. Within the degree of accuracy of fitting, these parameters coincided with the parameters obtained from the high-frequency semicircle in the Z*-plane (Table I). The left intercept of the high-frequency M*-plane semicircular fitting provided a capacitance matching with the low-frequency semicircular capacitive element (C_2) in the Z*-plane (Table I). The presence of a small depression angle $\theta_1^M(< 5^{\circ})$ in the high-frequency semicircle in the M*-plane is in agreement with that of the Z*-plane. The meaning of this depression angle (θ_1^M) is identical to that described earlier for θ_1. The activation energy of R_1^M is identical to that of R_1. With such a matching found between the two complex-plane (Z* and M*) representations, a suitable equivalent circuit can be constructed consisting of two R–C parallel elements connected in series. The temperature dependence of the M*-plane parameters (i.e. R_1^M, C_1^M, τ_1^M, θ_1^M) are identical to those obtained for the τ_1-relaxation in the Z*-plane. Therefore, interpretation for these parameters remains the same. The activation energies for the associated parameters are listed in Table II.

The semicircular feature of the low-frequency relaxation in the Y*-plane appears to be distorted toward the high-frequency region (Fig. 3). Careful analysis, however, yields a time constant, τ^Y, with an activation energy (E_{τ^Y}) 3.36 eV (Fig. 8). Its components R^Y and C^Y ($\tau^Y = R^Y C^Y$) also exhibit a temperature dependence (Fig. 9) with activation energies 2.48 eV (E_{R^Y}) for R^Y and 0.88 eV (E_{C^Y}) for C^Y. The sum of E_{R^Y} and E_{C^Y} is 3.36 eV, which is the same as E_{τ^Y}. As pointed out earlier, the τ^Y relaxation occurs in the frequency region corresponding to that of the low-frequency semicircular relaxation in the Z*-plane, and therefore may be attributed to a trapping effect (or space-charge polarization associated with the interfacial defects) at grain boundaries. This trapping effect is best represented by a series combination of a resistor and a capacitor [15–22, 33–35]. Considering this trapping in conjunction with the presence of large depression angle, θ^Y, which appears to decrease slightly with increasing temperature (Fig. 8b), the τ^Y relaxation may have resulted from a distribution of activation energies (or, relaxation times) with significant overlapping [36–38]. Although the origin of this overlapping is not clear at this time, the magnitude of depression angle

TABLE II Summary of the thermal activation energies (eV) for various parameters obtained from Z*-, M*- and Y*-plane relaxation measurements

E_{R_1}	E_{R_2}	E_{τ_1}	E_{τ_2}	$E_{R_1^M}$	$E_{\tau_1^M}$	E_{R^Y}	E_{C^Y}	E_{τ^Y}	E_{R_0}	$E_{R_1^Y}$
2.36	2.79	2.36	2.78	2.36	2.37	2.48	0.88	3.36	2.40	2.36

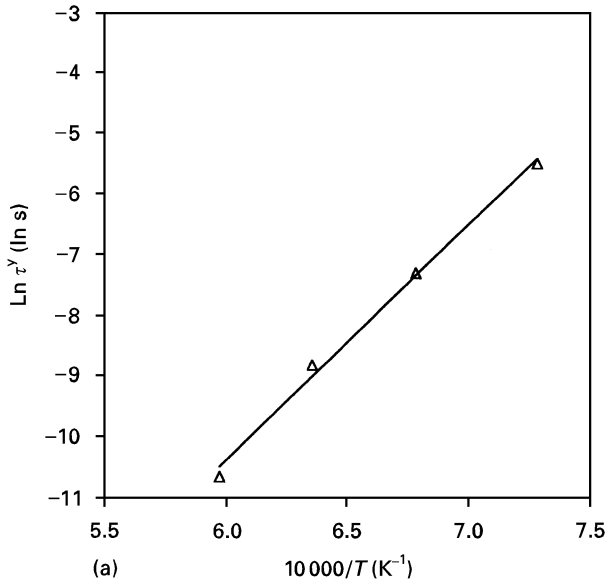

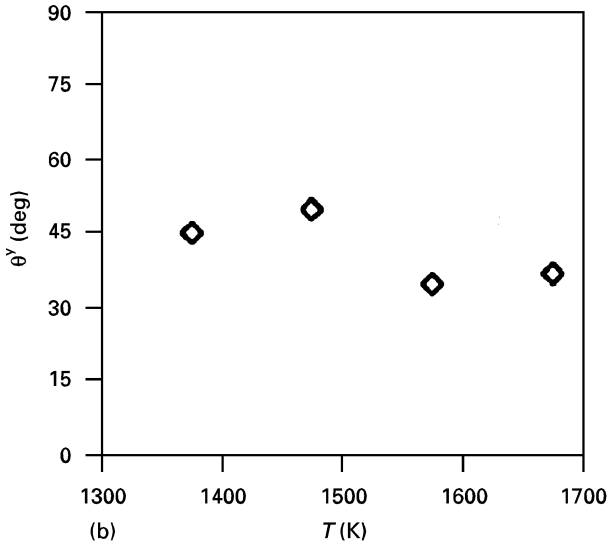

Figure 8 (a) Temperature dependence of τ^Y, showing an Arrhenius-type dependence. (b) The temperature dependence of the depression angle, θ^Y.

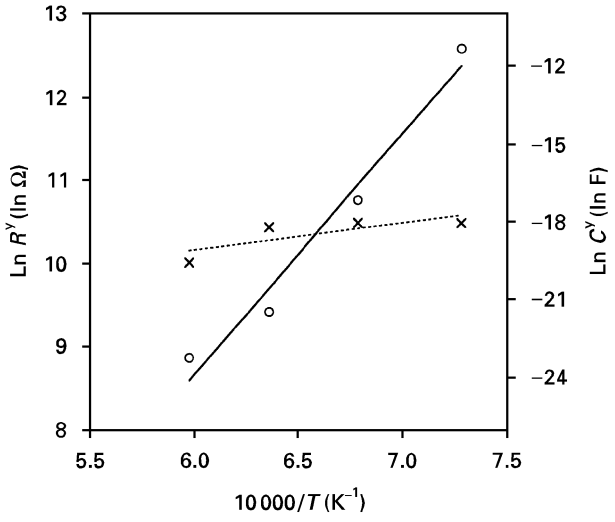

Figure 9 Temperature dependence of (○) the resistance, R^Y, and (×) capacitance, C^Y, associated with the low-frequency semicircular relaxation in the Y*-plane.

indicates a large heterogeneity in the trapping or charge transport processes across the grain-boundaries.

From the Y*-plane plot, other relevant electrical parameters were determined and are given in Table I. They are found to match those obtained from the Z*- and M*-planes. For example, the left intercept of the low-frequency semicircle in the Y*-plane corresponding to the d.c. resistance ($R_0 = R_{\text{d.c.}}$) of the material matches very closely with the sum of R_1 and R_2, obtained from the Z*-plane analysis. Also, the activation energy, E_{R_0}, of R_0 is found to be 2.40 eV, which is comparable to that of R_1, suggesting that the electrical conduction is governed by that in the grain interior rather than that in the grain boundary. On the other hand, the position of the vertical line upon extrapolation of the extreme high-frequency region in the Y*-plane yields R_1^Y, which is identical to the high-frequency relaxation resistance, R_1, in the Z*-plane. Finally, a Bode plot of the imaginary part of Y* (Fig. 10) indicates that the high-frequency limit of the

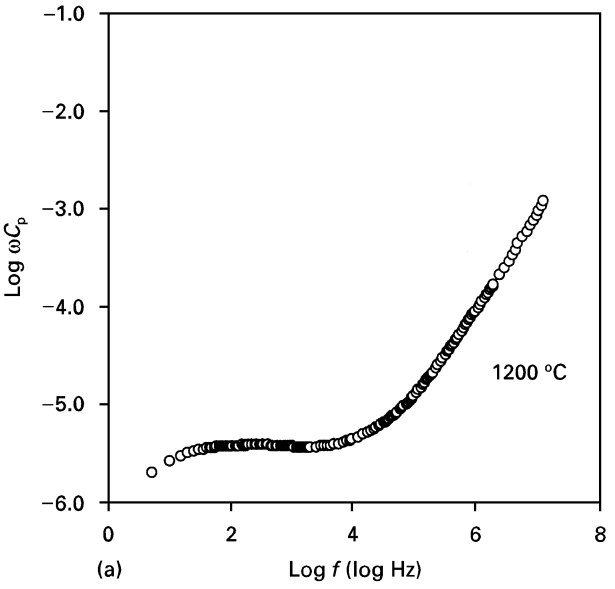

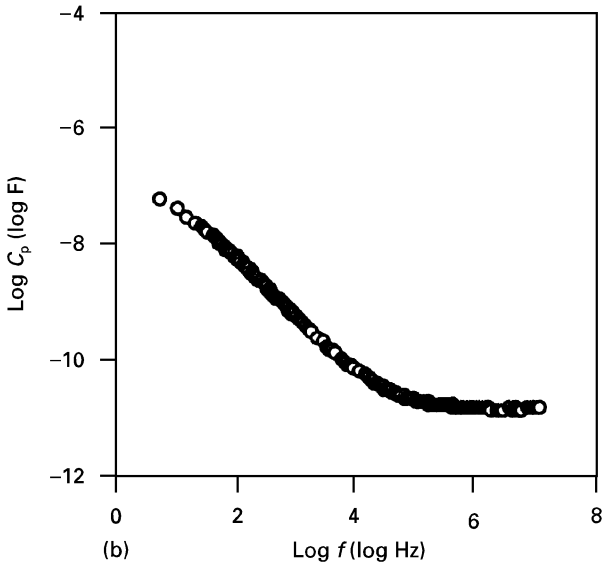

Figure 10 (a) The Bode plot of $Y''(\omega C_P)$. The linear region in the high-frequency limit yields C_∞, the high-frequency component of C_P which is independent of frequency, as shown in (b).

capacitance, C_∞, is about 14 pF. The value of C_∞ is insensitive to temperature and coincides with C_1 of the Z*-plane. A verification of the value of C_∞ is obtained in Fig. 10b. Both plots in Fig. 10 indicate a downward bending of the curve in the d.c. limit ($f \to 0$), excluding the possible contribution of space-charge effects typically found in ionic conductors [28, 29].

The foregoing discussion reveals two possible equivalent circuit representations of the a.c. electrical response of the undoped polycrystalline $CaZrO_3$. The equivalent circuit in Fig. 11a, extracted directly from the Z*-plane, consists of two parallel RC combinations in series. The equivalent circuit in Fig. 11b, extracted directly from the Y*-plane, consists of a d.c. resistance, R_0, and a high-frequency capacitance, C_∞, in parallel with an R–C series. As discussed earlier, the two circuits are equivalent in terms of their close correspondence between the two sets of circuit elements, and therefore both yield the same immittance at all frequencies. It should be noted, however, that while the equivalent circuit model depicted by Fig. 11a helps to delineate the individual contribution of grain and grain-boundary regions of a polycrystalline-based device, the circuit model of Fig. 11b serves to show a trapping effect which is not obviously seen from that of Fig. 11a. Similar dual equivalent circuit representation has been proposed previously for the yttria-based system [21, 22], an indication of the similarity between the two material systems as large band-gap polycrystalline oxides. Also, it is worth pointing out that a series R–C circuit model, like that in Fig. 11b, may become very useful in determining the spatial extension or distribution and level of interfacial traps, as demonstrated in the literature [33–35]. Finally, it should be noted that this type of multiplane analysis and, thus, the multiple equivalent circuit representation, conducted here and in the previous papers [21, 22] have been shown to be capable of obtaining relevant electrical parameters for each equivalent circuit independently, without resorting to any empirical distributed-element models. This is advantageous in cases where an exact mathematical relationship between the electrical parameters of different equivalent circuits is not readily obtainable, as is the case for many real material systems. This is particularly true when the dielectric response shows significant deviation from Debye behaviour and the depression angle shows appreciable temperature dependence (Fig. 8b).

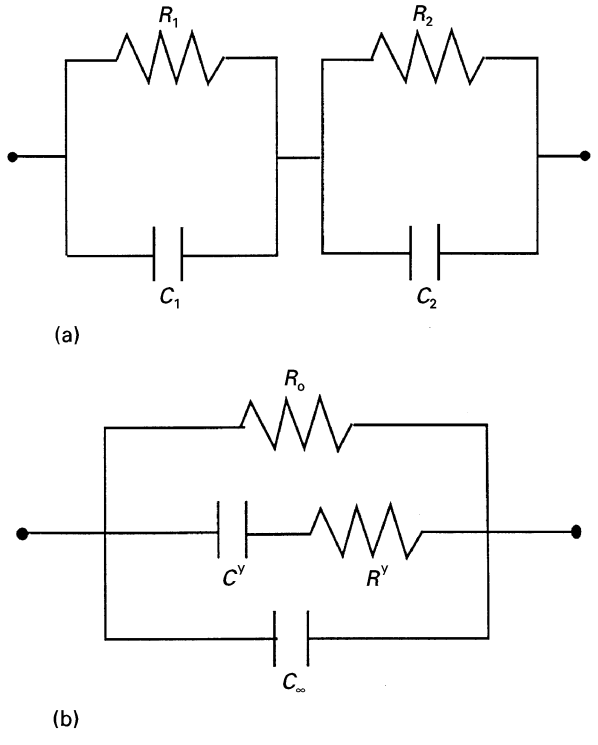

Figure 11 (a) Equivalent circuit model corresponding to the two semicircular relaxations in the impedance plane. R_1–C_1 and R_2–C_2 combinations constitute the high- and low-frequency relaxations, respectively. (b) Equivalent circuit representation of the a.c. electrical data analysed on the Y*-plane. The series combination of R^Y-C^Y constitutes the low-frequency relaxation. R_0 and C_∞ are the d.c. resistance and high-frequency limit ($f \to \infty$) capacitance, respectively.

5. Conclusion

The a.c. electrical behaviour of polycrystalline calcium zirconate, investigated in the temperature range 900–1400 °C in air, indicated two distinct relaxations in the Z*-plane. These relaxations are attributed to grain and grain-boundary contributions. The same a.c. electrical data showed a single-like relaxation process in the M*-plane due mainly to the influence of the high-frequency elements identified in the Z*-plane. This is merely a reflection of the dominant contribution of grains. The admittance plane analysis revealed the presence of a trapping effect, possibly associated with charge transport process across grain-boundaries.

Two possible equivalent circuit models have been proposed to represent the a.c. electrical response of the undoped polycrystalline $CaZrO_3$. The circuit elements for each equivalent circuit were extracted independently from the Z*- and Y*-planes. It has been demonstrated that these two circuit models are equivalent, but each portrays important physical process(es) not readily seen from one equivalent circuit representation alone.

Acknowledgements

This work was supported by a grant from the Edison Materials Technology Center (EMTEC) of the state of Ohio with matching funds from the Edward Orton Jr, Ceramic Foundation (Westerville, OH). Part of the modelling work was done under the NSF grant, DMR-9503429. M. A. Alim acknowledges the cooperative effort on behalf of The Ohio Brass Company for this work.

References

1. D. JANKE, *Metall. Trans.* **13B** (1982) 227.
2. C. WANG, X. XU and H.YU, *Solid State Ionics* **28–30** (1988) 542.
3. S. S. PANDIT, A. WEYL and D. JANKE, *ibid.* **69** (1994) 93.

4. T. YAJIMA, H. KAZEOKA, T. YOGO and H. IWAHARA, *ibid.* **47** (1991) 271.
5. T. YAJIMA, H. IWAHARA, K. KOIDE and K. YAMAMOTO, *Sensors Actuators B* **5** (1991) 145.
6. T. HIBINO, K. MIZUTANI, T. YAJIMA and H. IWAHARA, *Solid State Ionics* **57** (1992) 303.
7. A. de PRETIS, V. LONGO, F. RICCIARDIELLO and O. SBRAIZERO, *Silicates Industriels* **7–8** (1984) 139.
8. W. A. FISCHER, D. JANKE and M. SCHULENBURG, *Arch. Eisenhüttenw* **47** (1976) 51.
9. *Idem*, *ibid.* **47** (1976) 525.
10. D. JANKE, K. SCHWERDTFEGER, J. MACH and G. BOMBERG, *Stahl Eisen* **99** (1976) 1211.
11. M. A. SEITZ, *Int. J. Hybr. Microelec.* (*ISHM*) **3** (1980) 1.
12. J. J. ACKMANN and M. A. SEITZ, *CRC Crit. Rev. Biomed. Eng.* **11** (1984) 281.
13. S. H. CHU and M. A. SEITZ, *J. Solid State Chem.* **23** (1978) 297.
14. R. N. ESFAHANI and G. J. MACLAY, *J. Appl. Phys.* **67** (1990) 3409.
15. M. A. ALIM, *J. Am. Ceram. Soc.* **72** (1989) 28.
16. *Idem*, *Act. Pass. Elect. Comp.* **17** (1994) 99.
17. M. A. ALIM, M. A. SEITZ and R. W. HIRTHE, *J. Appl. Phys.* **63** (1988) 2337.
18. A. M. AZAD, L. B. YOUNKMAN, S. A. AKBAR and M. A. ALIM, *J. Am. Ceram. Soc.* **77** (1994) 481.
19. A. M. AZAD, S. A. AKBAR, L. B.YOUNKMAN and M. A. ALIM, *ibid.* **77** (1994) 3145.
20. C. C. CHEN, M. M. NASRALLAH, H. U. ANDERSON and M. A. ALIM, *J. Electrochem. Soc.* **142** (1995) 491.
21. V. D. PATTON, C. C. WANG, S. A. AKBAR and M. A. ALIM, *J. Appl. Phys.* **78** (1995) 1757.
22. C. C. WANG, V. D. PATTON, S. A. AKBAR and M. A. ALIM, *J. Mater. Res.* **11** (1996) 422.
23. H. J. DE BRUIN and S. P. S. BADWAL, *J. Aust. Ceram. Soc.* **14** (1978) 20.
24. *Idem*, *Phys. Status Solidi A* **49** (1978) K181.
25. J. F. McCANN and S. P. S. BADWAL, *J. Electrochem. Soc.* **129** (1982) 551.
26. J. B. BATES and J. C. WANG, *Solid State Ionics* **28–30** (1988) 115.
27. B. J. CHRISTENSEN, R. T. COVERDALE, R. A. OLSON, S. J. FORD, E. J. GARBOCZI, H. M. JENNINGS and T. O. MASON, *J. Am. Ceram. Soc.* **77** (1994) 2789.
28. A. K. JONSCHER, *J. Mater. Sci.* **13** (1978) 553.
29. A. K. JONSCHER, "Dielectric Relaxation in Solids" (Chelsea Dielectrics, London, 1983).
30. B. C. H. STEELE, B. E. POWELL and P. M. R. MOODY, *Proc. Br. Ceram. Soc.* **10** (1968) 87.
31. K. W. BROWALL, O. MULLER and R. H. DOREMUS, *Mater. Res. Bull.* **11** (1976) 1475.
32. C. C. WANG and S. A. AKBAR, The Edison Materials Technology Center (EMTEC) project CT-39 Final Report (1995).
33. J. R. MACDONALD, *J. Appl. Phys.* **62** (1987) R51.
34. J. MASERJIAN, *J. Vac. Sci. Technol.* **6** (1969) 843.
35. D. H. EATON and C. T. SAH, *Solid-State Electron.* **16** (1973) 841.
36. J. R. MACDONALD, *J. Appl. Phys.* **58** (1985) 1955.
37. *Idem*, *ibid.* **58** (1985) 1971.
38. I. D. RAISTRICK, J. R. MACDONALD and D. R. FRANCESHETTI, in "Impedance Spectroscopy: Empasizing Solid Materials and Systems", edited by J. R. MacDonald (Wiley, New York, 1987) p. 27.

Received 19 April
and accepted 17 September 1996